

# Simulating Time Evolution with Fully Optimized Single-Qubit Gates on Parameterized Quantum Circuits

Kaito Wada,<sup>1,\*</sup> Rudy Raymond,<sup>2,3</sup> Yu-ya Ohnishi,<sup>4,3</sup> Eriko Kaminishi,<sup>3,5</sup>  
Michihiko Sugawara,<sup>3</sup> Naoki Yamamoto,<sup>3,1</sup> and Hiroshi C. Watanabe<sup>3,†</sup>

<sup>1</sup>*Department of Applied Physics and Physico-Informatics, Keio University,  
3-14-1 Hiyoshi, Kohoku-ku, Yokohama, Kanagawa, 223-8522, Japan*

<sup>2</sup>*IBM Quantum, IBM Japan 19-21 Nihonbashi Hakozaki-cho, Chuo-ku, Tokyo, 103-8510, Japan*

<sup>3</sup>*Quantum Computing Center, Keio University, 3-14-1 Hiyoshi,  
Kohoku-ku, Yokohama, Kanagawa, 223-8522, Japan*

<sup>4</sup>*Materials Informatics Initiative, RD Technology & Digital Transformation Center,  
JSR Corporation, 3-103-9, Tonomachi, Kawasaki-ku,  
Kawasaki, Yokohama, Kanagawa, 210-0821, Japan*

<sup>5</sup>*JST PRESTO, 4-1-8 Honcho, Kawaguchi, Saitama 332-0012, Japan*

We propose a novel method to sequentially optimize arbitrary single-qubit gates in parameterized quantum circuits for simulating real and imaginary time evolution. The method utilizes full degrees of freedom of single-qubit gates and therefore can potentially obtain better performance. Specifically, it simultaneously optimizes both the axis and the angle of a single-qubit gate, while the known methods either optimize the angle with the axis fixed, or vice versa. Furthermore, we demonstrate how it can be extended to optimize a set of parameterized two-qubit gates with excitation-conservation constraints. We perform numerical experiments showing the power of the proposed method to find ground states of typical Hamiltonians with quantum imaginary time evolution using parameterized quantum circuits. In addition, we show the method can be applied to real time evolution and discuss the tradeoff between its simulation accuracy and hardware efficiency.

## I. INTRODUCTION

Quantum simulations of materials, which are becoming popular as promising applications of quantum computing, are practically useful in designing functional materials. One can track the time evolution of a quantum system by the real time evolution (RTE) algorithm, which is important to investigate, for example, the quantum dynamics under the irradiation of laser [1, 2]. In addition to the quantum phase estimation (QPE) algorithm [3, 4], and the variational quantum eigensolver (VQE) [5–7], the imaginary time evolution (ITE) algorithm [8, 9] might be applied to obtain the ground state energy and wavefunction. Although it is hard to run the QPE on current noisy intermediate-scale quantum devices, the VQE and ITE may be more realizable [5, 10–18]; actually several experimental studies on small systems have been reported [19, 20].

The basic ingredients for running quantum-classical hybrid algorithms are first to set a parameterized quantum circuit (PQC), sometimes called the trial wave function or simply the ansatz, and then to iteratively update its parameters by classical optimizers so that its final output state approximates the target state. The approximation accuracy of the target state achieved via quantum-classical hybrid algorithms heavily depends on the choice of PQC and the classical optimization strategy. Recent great efforts have revealed several essential

properties of the components of quantum-classical hybrid algorithms [21–23]. Among those literature works, we find interesting gradient-free optimizers that make full use of the specific parameterization of standard PQCs.

More precisely, those optimizers can analytically optimize a subset of the parameters at each iteration by exploiting the special type of analytic form of the cost function. Specifically, Nakanishi *et al.* [24] and Ostaszewski *et al.* [25] showed that the cost of VQE becomes a sinusoidal function of a single-qubit rotation, and thus we can determine the optimal rotational angle. Ostaszewski *et al.* also proposed a sequential optimization method for selecting the best rotational axes of qubits from the  $x$ ,  $y$ , or  $z$  rotations. Going further to relax the ansatz-dependency of VQE, a generalization of such gradient-free optimizers called the free-axis selection (or, Fraxis) [26] was proposed. The Fraxis algorithm analytically determines the best rotational axis for each single-qubit gate when the rotational angles are fixed.

In this article, with a particular attention to the task of simulating real and imaginary time evolution on a PQC, we make a further progress of this gradient-free optimization method. That is, for simulating time evolution we prove that both the rotational axis and angle of each single-qubit gate in the PQC can be analytically optimized in a coordinate-wise manner. This means that the PQC now acquires the ability for searching the quantum state in the Hilbert space that best approximates the time evolution in the coordinate-wise sense, and hence opening the new path to efficiently approximate the target state being driven via the time evolving propagators. Moreover, we show that this method can be applied to optimize some multi-qubit gates, in-

\* wkai1013keio840@keio.jp

† hcwatanabe@keio.jp

cluding the excitation-conserving two-qubit gates which play important roles in the quantum chemistry applications. We conducted numerical simulations of ITE for 1-dimensional (1D) Heisenberg model and  $H_2$  molecule, and showed that the proposed algorithm could approximate the target ground state faster and better than some previous methods. In addition, we also conducted numerical simulations of RTE for 1D Ising model using the proposed algorithms, and confirmed the reproduction of more accurate dynamics in our methods.

## II. METHODS

We first review the hardware-efficient objective function for time evolving simulation proposed by Benedetti *et al.* [27] and introduce a measure of hardware-efficiency of objective function. Then, we introduce *Free Quaternion Selection for Quantum Simulation* (abbreviated as **FQS**, where **QS** has two meanings: *Quaternion Selection* and *Quantum Simulation*), which can fully optimize an arbitrary single-qubit gate with hardware efficiency. Next, we show that the FQS can be extended to special multi-qubit gates such as the excitation-conserving gates.

### A. HARDWARE-EFFICIENT QUANTUM SIMULATION OF TIME EVOLUTION

Suppose a time evolution simulation based on the Hamiltonian given as  $\hat{H} = \sum_{k=1}^K h_k \hat{O}_k$ , where  $\hat{O}_k$  denotes a tensor product of Pauli operators for  $m$ -qubit  $\hat{O}_k \in \{\sigma_0 = I, \sigma_x, \sigma_y, \sigma_z\}^{\otimes m}$ ,  $h_k$  is a real valued coefficient, and  $K \sim \mathcal{O}(\text{poly}(m))$ . The time evolving propagator  $e^{-i\hat{H}t}$  is approximated with the first-order Trotter decomposition as

$$e^{-i\hat{H}t} = \left( e^{-i\hat{H}\Delta t} \right)^N \\ \simeq \left( e^{-ih_K \hat{O}_K \Delta t} \dots e^{-ih_k \hat{O}_k \Delta t} \dots e^{-ih_1 \hat{O}_1 \Delta t} \right)^N, \quad (1)$$

where  $N$  is the number of time steps and  $\Delta t \equiv t/N$ . Now a propagator  $e^{-ih_k \hat{O}_k \Delta t}$  is applied to an arbitrary state  $|\psi_{k-1}\rangle$ , which results in a state  $|\psi_k\rangle$  as

$$|\psi_k\rangle = e^{-ih_k \hat{O}_k \Delta t} |\psi_{k-1}\rangle. \quad (2)$$

Suppose an initial state  $|\psi_{k-1}\rangle$  is approximated by a PQC as  $U(\vec{\vartheta}_{[k-1]}^*) |\mathbf{0}\rangle$ , where  $\vec{\vartheta}_{[k-1]}^*$  is an optimal parameter set, and  $|\mathbf{0}\rangle$  is the computational basis state. Provided that a PQC has sufficient expressibility, there exists an optimal parameter set  $\vec{\vartheta}_{[k]}^*$  such that  $|\psi_k\rangle \simeq U(\vec{\vartheta}_{[k]}^*) |\mathbf{0}\rangle$ .

Therefore, a time evolution can be simulated if parameter sets that reproduce the time evolving propagator are somehow found. Hereafter, we focus on a series of processes to determine the  $k$ th optimal parameter set  $\vec{\vartheta}_{[k]}^*$  from  $\vec{\vartheta}_{[k-1]}^*$ . For readability, we write  $\vec{\vartheta}_{[k]}^*$  and  $\vec{\vartheta}_{[k-1]}^*$  as  $\vec{\vartheta}^*$ ,  $\vec{\vartheta}'$ , respectively, when it is obvious from the context. To determine the optimal parameter set  $\vec{\vartheta}^*$ , Benedetti *et al.* [27] proposed a recursive optimization using the objective function  $\mathcal{M}(\vec{\vartheta})$  based on the Euclidean distance as

$$\mathcal{M}(\vec{\vartheta}) \equiv \left\| U(\vec{\vartheta}) |\mathbf{0}\rangle - e^{-ih\hat{O}\Delta t} U(\vec{\vartheta}') |\mathbf{0}\rangle \right\|^2 \\ = 2 - 2\text{Re} \left[ \langle \mathbf{0} | U^\dagger(\vec{\vartheta}') e^{ih\hat{O}\Delta t} U(\vec{\vartheta}) |\mathbf{0}\rangle \right], \quad (3)$$

and

$$\vec{\vartheta}^* \equiv \underset{\vec{\vartheta} \in \Theta}{\text{argmin}} \mathcal{M}(\vec{\vartheta}) = \underset{\vec{\vartheta} \in \Theta}{\text{argmax}} \mathcal{F}(\vec{\vartheta}), \quad (4)$$

where  $\Theta$  is the parameter space, and  $\mathcal{F}(\vec{\vartheta})$  is defined as

$$\mathcal{F}(\vec{\vartheta}) \equiv \text{Re} \left[ \langle \mathbf{0} | U^\dagger(\vec{\vartheta}') e^{ih\hat{O}\Delta t} U(\vec{\vartheta}) |\mathbf{0}\rangle \right]. \quad (5)$$

Now we suppose a PQC  $U(\vec{\vartheta})$  consists of  $D$  parameterized single-qubit gates and arbitrary unitary gates without parameters such as CNOT gate. An element of the parameter space  $\Theta$  is given as  $\vec{\vartheta} = (\vartheta_1, \dots, \vartheta_D)$ , where  $\vartheta_d$  represents the parameters for the  $d$ th parameterized gate. To evaluate  $\mathcal{M}(\vec{\vartheta})$ , it is common to apply Hadamard tests with controlled gates for different parameters between  $\vec{\vartheta}$  and  $\vec{\vartheta}'$ . Because All  $D$  elements in  $\vec{\vartheta}$  usually differ from those in  $\vec{\vartheta}'$ , the Hadamard test requires additional  $\mathcal{O}(D)$  controlled gates and ancilla qubits, it may be difficult for near-term quantum devices when  $D$  is large.

The Hadamard test can be replaced by direct measurements as proposed by Mitarai *et al.* [28]. However, the direct measurements require more types of circuits, i.e., replacing  $D$  controlled gates with direct measurements incur the cost of evaluating  $\mathcal{O}(4^D)$  types of circuits.

To reduce the required quantum resources, it is possible to restrict the number of the gates to be updated in the objective function Eq. (5). On the other hand, such restricted updates may not be sufficient to minimize the simulation error  $\mathcal{M}(\vec{\vartheta})$  for  $e^{-ih\hat{O}\Delta t}$ . To balance between the hardware efficiency and simulation accuracy, we employ  $P \in \mathbb{N}$  *series of updates* procedure where parameterized gates are grouped into  $P$  sets, and the respective sets are represented by  $\Lambda_p$ , ( $p = 1, 2, \dots, P$ ). Here,  $\Lambda_p$  consists of the gate indices as  $\Lambda_p \subseteq \{1, 2, \dots, D\}$ . In the  $P$  series update, we divide the propagator into  $P$  terms maintaining total  $\Delta t$  time evolution. Although the division of  $\Delta t$  is not unique, we uniformly assign  $\Delta t/P$  similarly as [27]. Then, the original objective function in Eq. (5) is replaced by a series of the following objective functions

$$\mathcal{F}^{(p)}(\{\vartheta_d\}) \equiv \text{Re} \left[ \langle \mathbf{0} | U^\dagger(\vec{\vartheta}^{(p-1)}) e^{ih\hat{O}\Delta t/P} U(\{\vartheta_d\}; \vec{\vartheta}^{(p-1)}) | \mathbf{0} \rangle \right], \quad d \in \Lambda_p, \quad (6)$$

where  $\vec{\vartheta}^{(p-1)}$  denotes a parameter set whose  $\vartheta_d$ , ( $d \in \cup_{q=1}^{p-1} \Lambda_q$ ) have been updated from those in  $\vec{\vartheta}^{(0)} \equiv \vec{\vartheta}'$ . Here,  $U(\{\vartheta_d\}; \vec{\vartheta}^{(p-1)})$ ,  $d \in \Lambda_p$  denotes a PQC in which the elements of  $\Lambda_p$  are variable.  $\vec{\vartheta}^{(p)}$  is recursively obtained from  $\vec{\vartheta}^{(p-1)}$  by solving the following problems

$$\begin{aligned} \{\vartheta_d^*\} &= \underset{\{\vartheta_d\}}{\text{argmax}} \mathcal{F}^{(p)}(\{\vartheta_d\}), \quad d \in \Lambda_p, \\ \text{for } p &= 1, 2, \dots, P, \end{aligned} \quad (7)$$

where  $\vec{\vartheta}^{(p)}$  is defined by substituting  $\{\vartheta_d^*\}$ ,  $d \in \Lambda_p$  into  $\vec{\vartheta}^{(p-1)}$ . Eventually, we obtain the solution  $\vec{\vartheta}^* = \vec{\vartheta}^{(P)}$ , which approximates the state evolved by the propagator  $e^{-ih\hat{O}\Delta t}$  from the state with  $\vec{\vartheta}'$ . This update procedure are repeated for the total  $K$  Trotterized time propagators to simulate time evolution of  $\Delta t$  as in Eq. (1) and (2). The optimization method for Eq. (6) is not unique, and classical optimizers are conventionally employed, most of which update simultaneously multiple parameters with the cost of Hadamard tests consisting of multiple controlled gates and ancilla qubits. In the present study, instead, we employ coordinate-wise update, where parameters are sequentially updated for respective single-qubit gates.

Because there are at most  $|\Lambda_p|$  different parameterized gates between  $U^\dagger(\vec{\vartheta}^{(p-1)})$  and  $U(\{\vartheta_d\}; \vec{\vartheta}^{(p-1)})$ , the evaluation of the objective function Eq. (6) requires additional  $\mathcal{O}(|\Lambda_p|)$  controlled gates and one ancilla qubit. We introduce a hardware-efficiency measure  $\eta$  for an algorithm to simulate time evolution with Eq. (6) defined as

$$\eta \equiv \min_p \frac{1}{|\Lambda_p|}. \quad (8)$$

The measure varies in the range of  $1/D \leq \eta \leq 1$ ; in case of the lowest value  $\eta = 1/D$  the objective function in Eq. (6) is regressed to the original form in Eq. (5). On the other hand, in the highest value  $\eta = 1$ , namely, the most hardware-efficient case, the variables in each objective function are parameters of one single-qubit gate.

Note that the objective function in Eq. (6) does not prescribe any optimization methods and PQC structures. In general, it is important to employ a PQC with sufficient expressibility to describe the state of interest. While it is common to extend a quantum circuit by adding parameterized gates, the correlation among parameters emerges as a new obstacle for optimization upon increase of parameters. To circumvent this problem, it is required to both (1) simultaneously update correlating parameters and (2) construct a high-expressibility PQC with as fewer number of parameters as possible. To this

end, we propose a new optimization method for time evolution simulation by generalizing the free-axis selection (Fraxis) algorithm [26], which makes full use of degree of freedom with respect to a single-qubit gate. It is different from the previous work [27], where the objective function is analytically optimized for axis-fixed rotation gates by the analog of the NFT(Rotosolve) method. The three parameters of a single-qubit gate corresponds to a three-dimensional rotation which is best captured by the selection of *quaternion* system, and hence the name *free quaternion selection* of our proposed method.

In the next subsections, we firstly introduce the FQS formulation based on imaginary time evolution using the objective function for the most hardware-efficient case  $\eta = 1$ , where real time  $t$  is replaced by imaginary time  $\tau$  as  $t \rightarrow -i\tau$ . More specifically, in imaginary time evolution, a target state as in Eq. (2) becomes

$$\frac{1}{\sqrt{\mathcal{N}}} e^{-h\hat{O}\Delta\tau} U(\vec{\vartheta}') | \mathbf{0} \rangle, \quad (9)$$

where  $\Delta\tau \equiv \tau/N$ , and  $\mathcal{N}$  is a normalization factor as  $\mathcal{N} = \|e^{-h\hat{O}\Delta\tau} U(\vec{\vartheta}') | \mathbf{0} \rangle\|^2$ , which can be ignored in optimization problem of the objective function Eq. (5). In the Result section, we demonstrate the applications of imaginary time evolution for finding the ground state of the 1D Heisenberg model and  $H_2$  molecule.

Although we supposed  $\eta = 1$  and imaginary time evolution for simplicity in the following derivation, we emphasize that the FQS algorithm is neither limited to the most hardware-efficient objective functions of  $\eta = 1$  nor imaginary time evolution. Note that the FQS algorithm with  $\eta \neq 1$  is a simple extension of  $\eta = 1$  by using a coordinate-wise update for each general single-qubit gate in the same  $\Lambda_p$ . In particular, we also demonstrate the FQS application to simultaneous optimization for an excitation-conserving gate consisting of two parameterized single-qubit gates, and thus  $\eta = 1/2$ .

The appropriate hardware efficiency  $\eta$  should be determined from the trade-off between the performance of quantum devices and the required simulation accuracy. To demonstrate this point, we also applied FQS to real time evolution of the 1D Ising model with several hardware-efficiency levels.

## B. THE PROPOSED METHOD

### Free Quaternion Selection for Quantum Simulation

A general single-qubit gate with parameters of a rotational angle  $\theta$  and a rotational axis  $\mathbf{n}$  is written as

$$R_{\mathbf{n}}(\theta) \equiv e^{-i\frac{\theta}{2}\mathbf{n}\cdot\boldsymbol{\sigma}} = \cos\left(\frac{\theta}{2}\right)\sigma_0 - i\sin\left(\frac{\theta}{2}\right)\mathbf{n}\cdot\boldsymbol{\sigma}, \quad (10)$$

where  $\sigma_0$  is identity and  $\boldsymbol{\sigma} = (\sigma_x, \sigma_y, \sigma_z)$ . Here,  $\mathbf{n} = (n_x, n_y, n_z)$  denotes a normalized vector corresponding to the rotational axis. Suppose a PQC  $U(\vec{\vartheta})$  consisting of  $D$  general single-qubit gates. In the PQC, a parameter set  $\vartheta_d$  of the  $d$ th parameterized gate denotes

$$\vartheta_d = (\theta_d, \mathbf{n}_d) = (\theta_d, n_{dx}, n_{dy}, n_{dz}), \quad (11)$$

where  $\theta_d \in \mathbb{R}$  and  $\|\mathbf{n}_d\| = 1$ . For simplicity, we suppose the  $d$ th gate set  $\Lambda_d$  contains only the  $d$ th parameterized gate (i.e., the most hardware-efficient case  $\eta = 1$ ) and the total number of the gate sets is  $D$ . Then, the unitary operator with  $\Lambda_d$  in Eq. (6) is written as

$$U(\vartheta_d; \vec{\vartheta}^{(d-1)}) = V_2 R_{\mathbf{n}_d}(\theta_d) V_1, \quad (12)$$

where  $V_1$  and  $V_2$  denotes the unitary operators corresponding to the partial circuits prior and posterior to the  $R_{\mathbf{n}_d}$  in the PQC, respectively. Substituting Eq. (12) into Eq. (6) we obtain

$$\begin{aligned} \mathcal{F}^{(d)}(\theta_d, \mathbf{n}_d) &= \sqrt{g_0^2 + (\mathbf{n}_d \cdot \mathbf{g})^2} \\ &\times \sin\left[\frac{\theta_d}{2} + \arctan2(g_0, \mathbf{n}_d \cdot \mathbf{g})\right], \end{aligned} \quad (13)$$

where  $g_0$  and  $\mathbf{g} = (g_x, g_y, g_z)$  are defined as

$$\begin{aligned} g_\mu &\equiv \text{Re}\left[\langle \mathbf{0} | U^\dagger(\vec{\vartheta}^{(d-1)}) e^{-h\hat{O}\Delta\tau/D} V_2 \varsigma_\mu V_1 | \mathbf{0} \rangle\right] \\ &= \cosh\left(\frac{\Delta\tau}{D}h\right) \text{Re}\left[\text{tr}\left(\varsigma_\mu R_{\mathbf{n}'_d}^\dagger(\theta'_d)\rho'\right)\right] \\ &\quad - \sinh\left(\frac{\Delta\tau}{D}h\right) \text{Re}\left[\text{tr}\left(\hat{O}'\varsigma_\mu R_{\mathbf{n}'_d}^\dagger(\theta'_d)\rho'\right)\right], \end{aligned} \quad (14)$$

where  $\vartheta'_d = (\theta'_d, \mathbf{n}'_d)$  is the  $d$ th component of  $\vec{\vartheta}^{(d-1)}$ , and  $\varsigma_\mu \in \{\sigma_0, -i\sigma_x, -i\sigma_y, -i\sigma_z\}$  (See [29] for detailed derivation). Here, we used the following notations,

$$\hat{O}' \equiv V_2^\dagger \hat{O} V_2, \quad \rho' \equiv R_{\mathbf{n}'_d}(\theta'_d) V_1 | \mathbf{0} \rangle \langle \mathbf{0} | V_1^\dagger R_{\mathbf{n}'_d}^\dagger(\theta'_d). \quad (15)$$

Because the objective function Eq. (13) has sinusoidal form, the optimal parameter  $\vartheta_d^* = (\theta_d^*, \mathbf{n}_d^*)$  are trivially obtained as

$$\mathbf{n}_d^* = \frac{\mathbf{g}}{\|\mathbf{g}\|}, \quad \theta_d^* = \pi - 2\arctan2(g_0, \|\mathbf{g}\|) + 4l\pi, \quad (16)$$

---

### Algorithm 1 Imaginary Time Evolution with Free Quaternion Selection for Quantum Simulation

---

**Input** (1) Trotter-decomposed time propagators  $\{e^{-h_k\hat{O}_k\Delta\tau}\}_{k=1}^K$ , (2) a PQC  $U(\vec{\vartheta})$  with  $D$  general single-qubit gates,  $\vec{\vartheta} = (\vartheta_1, \dots, \vartheta_D)$ ,  $\vartheta_d = (\theta_d, \mathbf{n}_d) \in \mathbb{R}^4$ ,  $\|\mathbf{n}_d\| = 1$ , and (3) the number of time step  $N$ .

**Initialize** Choose initial gate parameters  $\vec{\vartheta}$ .

**repeat**

**for**  $k = 1, 2, \dots, K$  **do**

**for**  $d = 1, 2, \dots, D$  **do**

      Determine  $\mathcal{Q}_{+,0}, \mathcal{Q}_{\pm,x}, \mathcal{Q}_{\pm,y}, \mathcal{Q}_{\pm,z}$

      Set  $\mathcal{G}_d(\theta, \mathbf{n})$  by  $\mathcal{Q}_{+,0}, \mathcal{Q}_{\pm,x}, \mathcal{Q}_{\pm,y}, \mathcal{Q}_{\pm,z}$

**for**  $\mu = 0, x, y, z$  **do**

        Compute  $\varphi_\mu, \bar{\mathbf{n}}_\mu$

        Compute  $g_\mu = (g_0, \mathbf{g})$  from  $\vartheta_d, \mathcal{G}_d(\varphi_\mu, \bar{\mathbf{n}}_\mu)$

      Set  $\vartheta_d \leftarrow (\pi - 2\arctan2(g_0, \|\mathbf{g}\|), \mathbf{g}/\|\mathbf{g}\|)$

**until**  $N\Delta\tau$  time evolution

**Output** Gate parameters  $\vec{\vartheta}$

---

where we choose  $l \in \mathbb{Z}$  satisfying  $\theta_d^* \in [0, 4\pi]$ . Thus, the optimal value of  $\vartheta_d^*$  can be determined from  $g_\mu$ .

The first term in Eq. (14) can be determined by a parameter  $\vartheta'_d = (\theta'_d, \mathbf{n}'_d)$  without quantum computation as (See [29] for derivation)

$$\text{Re}\left[\text{tr}\left(\varsigma_\mu R_{\mathbf{n}'_d}^\dagger(\theta'_d)\rho'\right)\right] = \begin{cases} \cos(\theta'_d/2), & \mu = 0 \\ n'_{d\mu} \sin(\theta'_d/2), & \mu \neq 0 \end{cases}. \quad (17)$$

On the other hand, quantum computations are required for the second term of Eq. (14). In general, the evaluation of the second terms requires four types of measurements in total using the Hadamard test with controlled operation on  $\varsigma_\mu R_{\mathbf{n}'_d}^\dagger(\theta'_d)$ . For  $\eta = 1$ , however, we can replace the Hadamard test with modest number of direct measurements.

In the following part of this section, we describe the details of the direct measurement protocol. First, we note  $\varsigma_\mu R_{\mathbf{n}'_d}^\dagger(\theta'_d)$  in the second term of Eq. (14) can be transformed into single-qubit gate as  $R_{\bar{\mathbf{n}}_\mu}(\varphi_\mu)$ , where  $\varphi_\mu$  and  $\bar{\mathbf{n}}_\mu$  are determined with  $\theta'$  and  $\mathbf{n}'_d$  that are obtained in the previous processes as for  $\mu = 0$

$$\varphi_0 = -\theta'_d, \quad \bar{\mathbf{n}}_0 = \mathbf{n}'_d, \quad (18)$$

and for  $\mu \neq 0$

$$\begin{aligned} \varphi_\mu &= 2\arctan2\left(\sqrt{1 - n'_{d\mu} \sin^2\left(\frac{\theta'_d}{2}\right)}, n'_{d\mu} \sin\left(\frac{\theta'_d}{2}\right)\right), \\ \bar{n}_{\mu t} &= \frac{1}{\sqrt{1 - n'^2_{d\mu} \sin^2\left(\frac{\theta'_d}{2}\right)}} \\ &\quad \times \left(\cos\left(\frac{\theta'_d}{2}\right)\delta_{\mu t} - \sin\left(\frac{\theta'_d}{2}\right)\sum_{s=x,y,z}\epsilon_{\mu st}n'_{ds}\right), \\ t &= x, y, z, \end{aligned} \quad (19)$$

where  $\delta_{\mu t}$  and  $\epsilon_{\mu st}$  denotes the Kronecker delta and the three-dimensional Levi-Civita symbol, respectively [29]. Next, we define a generator  $\mathcal{G}_d$  as a function of rotation angle  $\theta$  and axis  $\mathbf{n}$

$$\mathcal{G}_d(\theta, \mathbf{n}) \equiv \text{Re}\left[\text{tr}\left(\hat{O}'R_{\mathbf{n}}(\theta)\rho'\right)\right] \quad (20)$$

Furthermore, the generator is transformed as

$$\begin{aligned} \mathcal{G}_d(\theta, \mathbf{n}) &= \cos\left(\frac{\theta}{2}\right)\mathcal{Q}_{+,0} \\ &\quad + \sin\left(\frac{\theta}{2}\right)\sum_{s=x,y,z}n_s\frac{(\mathcal{Q}_{+,s} - \mathcal{Q}_{-,s})}{2}, \end{aligned} \quad (21)$$

where

$$\mathcal{Q}_{\pm,\nu} \equiv \text{tr}\left(\hat{O}'e^{\mp i\sigma_\nu\pi/4}\rho'e^{\pm i\sigma_\nu\pi/4}\right), \quad \nu = 0, x, y, z. \quad (22)$$

Note that  $\mathcal{Q}_{\pm,\nu}$  is independent of  $(\theta, \mathbf{n})$  and can be evaluated by direct measurement with a PQC, where a single-qubit gate  $e^{\mp i\sigma_\mu\pi/4}$  is inserted after the gate of interest. The generator agrees with the second term in Eq. (14) when  $(\varphi_\mu, \bar{\mathbf{n}}_\mu)$  is substituted into  $(\theta, \mathbf{n})$ . Hence, once  $\mathcal{Q}_{+,0}$ ,  $\mathcal{Q}_{\pm,x}$ ,  $\mathcal{Q}_{\pm,y}$ ,  $\mathcal{Q}_{\pm,z}$  are obtained for the  $d$ th gate, we can evaluate the second term in Eq. (14) without additional quantum computation as shown in Algorithm 1. Therefore, the optimal values of single-qubit gate parameters can be analytically determined with only seven types of expectation values in the direct measurement scheme: no ancilla qubits, no additional CNOT gates, which is rather advantageous on present real devices with

limited qubit connectivity and significant error from control operation. Therefore, we believe the direct measurement scheme of FQS as the one of the most hardware-efficient protocol for time evolving simulation.

In the following, for simplicity we refer to the algorithm described in this section as FQS(1q, 3p), where the 1q denotes its targeting parameterized single-qubit gates, and the 3p denotes the full parameterization of each gate: the (*unit*) *quaternion* which can be identified with a set of rotational angle and axis or direct parameters of a single-qubit gate [30]. We emphasize the fact that all parameters of a single-qubit gate are simultaneously optimized in FQS(1q, 3p). Thus, the time evolution is more accurately simulated by making full use of expressibility of a target gate. Obviously, FQS can be used to optimize the specific single-qubit gates such as rotation gates with fixed axis (i.e., NFT [24] or Roto-solve [25]) and the Fraxis [26] gate, which is equivalent to  $R_{\mathbf{n}}(\pi)$ . For simplicity, we also refer to the FQS(1q, 1p) and the FQS(1q, 2p) as NFT and Fraxis, respectively.

### Free quaternion selection for multi-qubit gate

Here, we extend the FQS to special multi-qubit gates that can be decomposed as

$$A \cdot R_{\mathbf{n}}(\theta) \cdot B \cdot R_{\mathbf{n}}^\dagger(\theta) \cdot C, \quad (23)$$

where  $A$ ,  $B$ , and  $C$  denote arbitrary unitary gates without parameters (such as the CNOT and Pauli gates), and  $R$  and  $R^\dagger$  share the same parameter  $\vartheta = (\theta, \mathbf{n})$ . Table I lists some examples of the well-known gates in this class. They are excitation-conserving, swap, Hop, and Reconfigurable Beam Splitter (RBS) gates.

Because  $R_{\mathbf{n}}(\theta)$  and  $R_{\mathbf{n}}^\dagger(\theta)$  gates share the same parameters in those multi-qubit gates, these gates are simultaneously updated with an optimization scheme similar to the FQS method. In this case, each  $\Lambda$  includes two single-qubit gates making the hardware-efficiency measure  $\eta \leq 1/2$ . Although in the following, we suppose the simple case that each  $\Lambda_p$  consists of only two single-qubit gates, namely  $\eta = 1/2$  ( $|\Lambda_p| = 2$ ,  $\forall p = 1, 2, \dots, P$ ), with shared parameters which are written as  $\vartheta_p = (\theta_p, \mathbf{n}_p)$ , it is straightforward to generalize it to  $|\Lambda| > 2$  by using a coordinate-wise update with a multi-qubit gate in Eq. (23).

Given the excitation-conserving gate in Table I, the objective function for the  $p$ th gate set is rewritten by substituting Eq. (23) and  $\theta = \pi$  into Eq. (6) as

$$\begin{aligned} \mathcal{F}^{(p)}(\pi, \mathbf{n}_p) &= \text{Re}\left[\langle \mathbf{0} | U^\dagger(\vec{\vartheta}^{(p-1)})e^{-h\hat{O}\Delta\tau/P}V_2AR_{\mathbf{n}_p}(\pi)BR_{\mathbf{n}_p}^\dagger(\pi)CV_1 | \mathbf{0} \rangle\right] \\ &= \sum_{s,t=x,y,z}n_{ps}n_{pt}\text{Re}\left[\langle \mathbf{0} | U^\dagger(\vec{\vartheta}^{(p-1)})e^{-h\hat{O}\Delta\tau/P}V_2A\sigma_tB\sigma_sCV_1 | \mathbf{0} \rangle\right], \end{aligned} \quad (24)$$

TABLE I. Examples of the special two-qubit gates in the form of  $AR_n(\theta)BR_n^\dagger(\theta)C$ . The parameterized single-qubit gate  $R_n(\theta)$  is supposed to act on the second qubit (more precisely,  $R_n(\theta)$  denotes  $I_1 \otimes R_n(\theta)$ ). The arbitrary gates  $A$ ,  $B$ , and  $C$  without parameters are represented by  $Z_2$  (Pauli Z),  $X_{i,j}^c$  (CNOT),  $Z_{i,j}^c$  (CZ) gates, and their products, where the superscript  $c$  represents a controlled-gate with the first (control) and second (target) subscripts. In the right-most column, the direct sum of matrices  $1 \oplus \mathbf{M} \oplus \pm 1$  denotes the block diagonal matrix  $\text{Diag}(1, \mathbf{M}, \pm 1)$ .

Gate Type	$A$	$B$	$C$	$R_n(\theta)$	$AR_n(\theta)BR_n^\dagger(\theta)C$
excitation-conserving <sup>a</sup>	$X_{2,1}^c$	$Z_{1,2}^c$	$X_{2,1}^c$	$\theta = \pi$ $\mathbf{n}(\psi, \phi)$	$1 \oplus \begin{pmatrix} -\cos \psi & e^{i\phi} \sin \psi \\ e^{-i\phi} \sin \psi & \cos \psi \end{pmatrix} \oplus 1$
swap	$X_{2,1}^c$	$X_{1,2}^c$	$X_{2,1}^c$	$\theta$ $\mathbf{n} = (0, 0, 1)$	$1 \oplus \begin{pmatrix} 0 & e^{i\theta} \\ e^{-i\theta} & 0 \end{pmatrix} \oplus 1$
Hop	$Z_2 X_{2,1}^c$	$Z_{1,2}^c$	$X_{2,1}^c$	$\theta = \pi$ $\mathbf{n}(\psi, \phi = 0)$	$1 \oplus \begin{pmatrix} \cos \psi & -\sin \psi \\ \sin \psi & \cos \psi \end{pmatrix} \oplus -1$
RBS	$X_{2,1}^c$	$Z_{1,2}^c$	$X_{2,1}^c Z_2 Z_{1,2}^c$	$\theta = \pi$ $\mathbf{n}(\psi, \phi = 0)$	$1 \oplus \begin{pmatrix} \cos \psi & \sin \psi \\ -\sin \psi & \cos \psi \end{pmatrix} \oplus 1$

<sup>a</sup> excitation-conserving gate with 2 parameters  $(\psi, \phi)$  are represented by the polar coordinate of the rotational axis  $\mathbf{n}$  such as  $\mathbf{n}(\psi, \phi) = (\sin(\psi/2) \cos(\phi), \sin(\psi/2) \sin(\phi), \cos(\psi/2))$ .

where  $V_1$  and  $V_2$  denotes the parts of the PQC as in the previous subsection. By definition of a  $3 \times 3$  asymmetric matrix  $G^{(p)}$  as

$$G_{st}^{(p)} \equiv \text{Re} \left[ \langle \mathbf{0} | U^\dagger (\vec{\vartheta}^{(p-1)}) e^{-h\hat{O}\Delta\tau/P} V_2 A \sigma_t B \sigma_s C V_1 | \mathbf{0} \rangle \right],$$

$$s, t \in \{x, y, z\}, \quad (25)$$

Eq. (24) is transformed in a quadratic form as

$$\mathcal{F}^{(p)}(\pi, \mathbf{n}_p) = \mathbf{n}_p^T G^{(p)} \mathbf{n}_p, \quad (26)$$

where superscript  $T$  denotes a transpose operation. The optimal value can be computed from the symmetric matrix  $S^{(p)}$ , defined as  $S^{(p)} \equiv (G^{(p)} + (G^{(p)})^T)/2$ , so that the optimal parameter becomes

$$\mathbf{n}_p^* = \underset{\mathbf{n}_p}{\text{argmax}} \mathbf{n}_p^T S^{(p)} \mathbf{n}_p, \quad (27)$$

where the eigenvector corresponding to the largest eigenvalue of  $S^{(p)}$  is the analytical solution. As for the objective function Eq. (6) with respect to Swap, Hop, or RBS gates, we also derive the analytical optimization form as in [29].

To obtain a solution of Eq. (27), we need to evaluate the elements of  $G^{(p)}$  in Eq. (25), which can be written in an unified expression similarly to the previous subsection, as

$$\text{Re} \left[ \langle \mathbf{0} | U^\dagger (\vec{\vartheta}^{(p-1)}) e^{-h\hat{O}\Delta\tau/P} \right. \\ \left. \times W_A R_{\bar{\mathbf{n}}_2}(\varphi_2) W_B R_{\bar{\mathbf{n}}_1}(\varphi_1) W_C | \mathbf{0} \rangle \right], \quad (28)$$

where  $W_A$ ,  $W_B$ , and  $W_C$  are defined as

$$W_A = V_2 A, \quad W_B = R_{\mathbf{n}'_p}(\theta'_p) B R_{\mathbf{n}'_p}^\dagger(\theta'_p), \quad W_C = C V_1. \quad (29)$$

Note that  $(\varphi_1, \bar{\mathbf{n}}_1)$ ,  $(\varphi_2, \bar{\mathbf{n}}_2)$  are determined by each element of  $G^{(p)}$  as in the previous subsection. In addition, an analytical solution of the objective function for Swap, Hop, or RBS gates also requires quantities in the same form as Eq. (28). In principle, these quantities in Eq. (28) can be evaluated with Hadamard test with two control operations on  $R_{\bar{\mathbf{n}}_2}(\varphi_2)$  and  $R_{\bar{\mathbf{n}}_1}(\varphi_1)$ . However, direct measurements without ancilla qubits and CNOT gates are available similarly as proposed in literature [28].

Here, we denote the FQS method for optimizing Eq. (27) as *FQS with  $u$ -qubit gates of 2 parameters*;  $\text{FQS}(uq, 2p)$ , where  $u$  is the number of qubits subject to nontrivial action of  $A$ ,  $B$ , and  $C$ . On the other hand, the FQS method to optimize only one degree of freedom out of three in  $\vartheta_p = (\theta_p, \mathbf{n}(\psi_p, \phi_p))$  is termed *FQS with  $u$ -qubit gates of 1 parameter*;  $\text{FQS}(uq, 1p)$ , which can be applied to Hop, RBS, swap, and the excitation-conserving gate with one fixed degree of freedom.

In contrast to the conventional excitation-conserving gate where only rotational angle  $\psi$  is the optimization target, the  $\text{FQS}(2q, 2p)$  can simultaneously update not only  $\psi$  but also  $\phi$ , which seems to be advantageous to exhibit higher expressibility and to avoid local minimum and saddle points. To verify this feature, we also carry out controlled experiments where the two parameters  $\psi, \phi$  of an excitation-conserving gate are sequentially and separately optimized.

### III. RESULTS AND DISCUSSION

In this section, we verify the performance of the proposed FQS methods in real and imaginary time simulations of typical Hamiltonians. The ITE simulations were executed with  $\eta = 1$  to find the ground state of the 1D Heisenberg model and  $\text{H}_2$  molecule. As for real time evolution, we simulated the 1D Ising model with various hardware-efficiency. All simulations presented in the paper were carried out using statevector simulator of Qiskit [31]. The settings of each experiments are detailed in [29].

#### A. 1D HEISENBERG MODEL WITH FQS(1Q, 3P)

Here, we consider a 5-qubit 1D Heisenberg model under the periodic boundary condition. The Hamiltonian is given as

$$H = J \sum_{(i,j) \in E} (X_i X_j + Y_i Y_j + Z_i Z_j) + h \sum_{i \in V} Z_i, \quad (30)$$

where the coupling constant  $J$  and the external fields  $h$  satisfy  $J = h = 1$ , and  $G = \{V, E\}$  is the undirected graph of the lattice with 5 nodes. The imaginary time propagators were prepared under the first-order Trotter decomposition with fixed time step  $\Delta\tau = 0.50$ .

The advantage of FQS is its simultaneous optimization of multi parameters. To confirm it, we carried out 30 independent ITE simulations for the Hamiltonian in Eq. (30) with different initial parameters, which were randomly generated. We employed a 2-layer ansatz with ladder-like entangler, where one parameterized single-qubit gate is placed at each qubit in the layer.

For fair comparison, we prepared two settings such that two simulations were performed on PQC with equivalent expressibility. In the first condition (Setting-A), all  $D = 15$  single-qubit gates  $U_d(\vartheta)$  in the ansatz were treated by FQS(1q, 3p). On the other hand, in the second condition (Setting-B), these 15 gates were decomposed into 15  $R_y$  and 30  $R_z$  gates ( $D = 45$ ) as  $U(\vartheta) = R_z(\phi)R_y(\psi)R_z(\lambda)$ , and the 45 gates were sequentially optimized with NFT.

Figure 1 shows the cumulative distributions of the fidelity between the ground state and the resulting state at 40, 80, 160, and 320 time step. It is obvious that FQS reproduced ITE paths more accurately than NFT, which shows the importance to simultaneously optimize multiple parameters. It should be also noted that NFT and FQS(1q, 3p) require three and seven types measurements per gate update, respectively (see Section II-B). As a result, the NFT optimization of a general single-qubit gate requires nine measurement types because the gate is decomposed into three fixed-axis rotation gates, e.g., one  $R_y$  and two  $R_z$  gates. Therefore, the computational cost for a general single-qubit gate by FQS(1q, 3p), which requires seven measurement types, is actually smaller than that of NFT while achieving higher accuracy due to taking into account correlation among parameters.

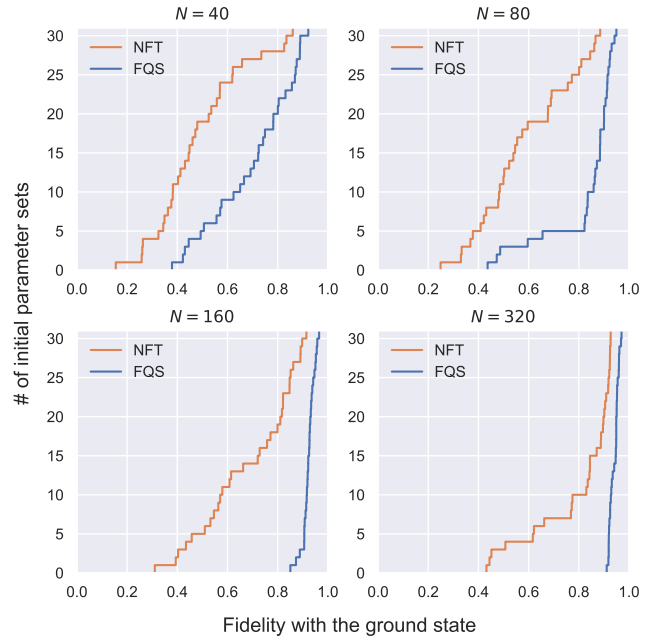


FIG. 1. Cumulative distributions of the fidelity between the ground state and the imaginary time evolved state in 1D Heisenberg model. Orange and blue lines represent the cumulative distributions of NFT and FQS(1q, 3p), respectively.

#### B. $\text{H}_2$ MOLECULE WITH FQS(2Q, 2P)

In this section, we confirm performance of the FQS for excitation-conserving gates useful for quantum chemical calculation. We chose  $\text{H}_2$  molecule with the atomic distance of 0.74 Å as a benchmark system, where the molecular Hamiltonian obtained by Hartree-Fock method with STO-3G basis was mapped to 4-qubit Hamiltonian by Jordan-Wigner transformation. The imaginary time propagators were prepared as well as in the previous section with fixed time step  $\Delta\tau = 1.0$ . In this section, we employed an ansatz with a cascade of the 5 excitation-conserving gates  $N_i(\psi_i, \phi_i)$ , ( $i = 1, 2, \dots, 5$ ).

When compared to the Hop and RBS gates, the excitation-conserving gate has an additional degree of freedom, which allows to express relative phase in complex space. However, the advantage is not unveiled trivially in treatment of molecular Hamiltonian. This is because the eigenstates can be represented by vectors in real space. To confirm this point, we compared two ITE simulations, where  $\psi$  and  $\phi$  are variable for FQS(2q, 2p), while  $\phi = \pi$  for FQS(2q, 1p). Here, we refer the simulation conditions for FQS(2q, 1p) and FQS(2q, 2p) as Setting-C and -D, respectively, (See Table I). For FQS(2q, 2p) simulations we randomly chose the initial value of  $\phi$ . On the other hand, FQS(2q, 1p) and FQS(2q, 2p) shared the same initial values of  $\psi$ , which were randomly generated.

Figure 3(a) shows all simulations started from the similar energy level, which implies the initial states contain the ground state with amplitude in the same scale. Note

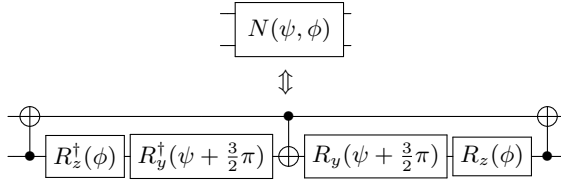


FIG. 2. Decomposition of the excitation-conserving gate  $N(\psi, \phi)$  using  $R_y$  and  $R_z$  gates.

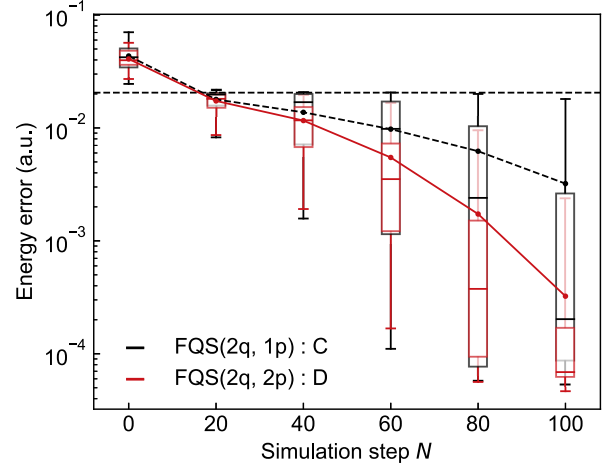
that FQS(2q, 1p) with  $\phi = \pi$  reached to the chemical accuracy ( $\Delta E = 10^{-3}$  a.u.) in the best case. However, in the worst case of FQS(2q, 1p), the energy was not improved from the HF level, which implies that the expressibility for the ground state does not necessarily guarantee sufficient expressibility to reproduce accurate ITE path. In contrast, FQS(2q, 2p) initiating from a state in complex space outperformed FQS(2q, 1p) with  $\phi = \pi$ . This is presumably because FQS initiating from complex vector can make use of larger Hilbert space which includes not only complex space represented by  $\phi \neq \pi$  but also extended real space caused by the phase cancellation among  $\phi$ 's in excitation-conserving gates. Thus, the time evolution in FQS can possibly be described better with  $\phi \neq \pi$ .

Next, we evaluated the correlation of two parameters  $(\psi, \phi)$  in each excitation-conserving gate. To this end, we decomposed an excitation-conserving gate into  $R_y$  and  $R_z$  gates as Fig. 2 according to [32]. Then we sequentially updated  $\psi$  and  $\phi$  with FQS(2q, 1p) in different gate sets (Setting-F). Since these multiple  $R_y$  and  $R_z$  gates share the parameters  $\psi$  and  $\phi$ , respectively, required controlled operations still remain two for one excitation-conserving gate, namely  $\eta = 0.5$ , even after the gate decomposition. On the other hand, the number of optimization is doubled as  $P = 10$ , which can lead to overestimation of its performance through scaling effect of the propagator  $e^{-ih\hat{O}\Delta t/P}$  in Eq. (6). Hence, for fair comparison with FQS(2q, 1p) and FQS(2q, 2p), we carried out *twice sweep update* for each optimization of Eq. (6) in the FQS(2q, 2p) method, where we employed  $P = 10$  allowing overlap of  $\Lambda$ . We refer this simulation condition as Setting-E.

For statistical accuracy, we independently conducted 20 ITE simulations by using randomly-generated common initial states for both FQS(2p, 1p) and FQS(2q, 2p) methods. Figure 3 showed a boxplot of the energy in course of simulation time, which exhibits distinct difference where FQS(2q, 2p) reached to lower energy states when compared to FQS(2q, 1p). This discrepancy implies the importance of taking into account correlation between  $\psi$  and  $\phi$ .

FQS(2q, 2p) requires eight-type measurements to evaluate Eq. (28), because  $G_{xy} = -G_{yx}$  holds for the excitation-conserving gate. On the other hand, four-type measurements are required in FQS(2q, 1p) for the respective gates. Therefore, the number of required measure-

(a) Applications to excitation-conserving gate



(b) Consistent number of optimizations per one propagator

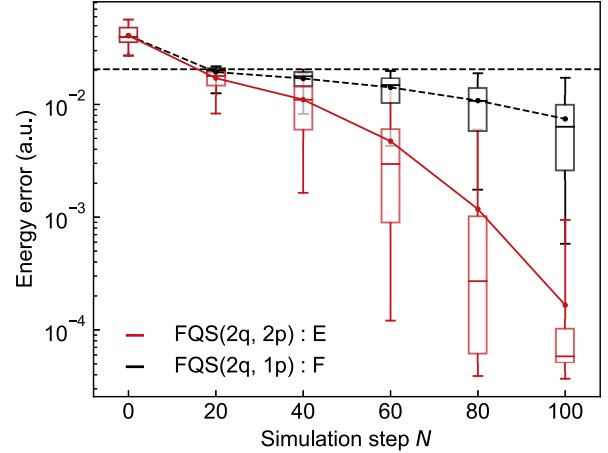


FIG. 3. Energy in the course of simulation steps  $N$  with  $\Delta\tau = 1$ . Black and red lines correspond to the results of FQS(2q, 1p) and FQS(2q, 2p), respectively. Box and whisker plot denote quantiles obtained from the ITE simulation results with 20 different initial parameter sets. Dash line represents the HF energy level.

ments for a single excitation-conserving gate in Eq. (23) with FQS(2q, 2p) is equivalent to that in separate optimization with FQS(2q, 1p).

Considering the twice sweep, FQS(2q, 2p) simulation in Fig. 3(b) are twice as expensive with respect to the measurement cost. To evaluate the simulation accuracy with consistent measurement cost, FQS(2p, 1p) with Setting-F should be compared with FQS(2q, 2p) with Setting-D. Eight types of measurements are required in both simulations. As shown in Fig. 3, notably, the performance of FQS(2q, 2p) (Setting-D) was almost retained in this case when compared to the twice-sweep simula-

tion (Setting-E) in Fig. 3(b), although the worst case in single sweep resulted in slightly larger energy. Altogether, the FQS(2q, 2p) application to the excitation-conserving gate realizes incorporation of the parameter correlation without any additional cost when compared to FQS(2q, 1p), which remarkably outweighs the time scaling of the propagator according to the number of the parameterized gates.

### C. REAL TIME EVOLUTION FOR 1D ISING MODEL WITH FQS(1Q, 3P)

We applied FQS algorithm to real time evolution of a 4-qubit 1D Ising model with transverse-field under the open boundary condition. The Hamiltonian is given as

$$H = -J \sum_{i=0}^{N-2} Z_i Z_{i+1} - h \sum_{i=0}^{N-1} X_i, \quad (31)$$

where  $J = h = 1$ . We employed the ground state  $|0\rangle^{\otimes 4}$  of the Hamiltonian without transverse-field as the initial state at  $t = 0$ . The time propagators were prepared using the first-order Trotter decomposition with fixed time step  $\Delta t = 0.01$ . We used the 2-layer PQC with a linear entangler, where each qubit in the layer has one single-qubit gate, and the single-qubit gate  $U_d$  is a general single-qubit gate in FQS and  $R_x$ - $R_y$ - $R_z$  gates in NFT so that FQS and NFT simulations were performed on PQC with equivalent expressibility as in the previous section.

In order to demonstrate the trade-off between simulation accuracy and hardware efficiency, we prepared several simulation settings with different values of hardware efficiency  $\eta$ . In the most hardware-efficient case ( $\eta = 1$ ), a propagator is divided by the total number of single-qubit gates  $D$ , and the respective single-qubit gates are updated according to Eq. (6) with respect to a divided propagator  $e^{-ih_k \hat{O}_k \Delta t / D}$ , where  $D = 12$  in FQS and  $D = 36$  in NFT.

As the next hardware-efficient case, we employed a group update for a propagator of  $e^{-ih_k \hat{O}_k \Delta t / P}$  with the objective function in Eq. (6). Here, the respective gate sets  $\Lambda_p$ , ( $p = 1, \dots, P$ ) consist of single-qubit gates in identical layers ( $|\Lambda| = m$  and Hardware efficiency  $\eta = 1/m$ , where  $m$  is the number of qubits). Then, in the respective optimizations, we conducted FQS algorithm  $|\Lambda|$  times in coordinate-wise fashion.

For comparison, we also carried out the simulations of  $\eta = 1/D$  using either NFT or FQS(1q, 3p), where all parameterized gates are sequentially updated to approximate the action of one propagator  $e^{-ih_k \hat{O}_k \Delta t}$ . We refer to such simulations as NFT(All) and FQS(All).

Figure 4 shows total magnetization per site  $\langle N^{-1} \sum_i Z_i \rangle$  and infidelity at each time step with different levels of hardware-efficiency, where the infidelity is defined as

$$1 - \|\langle \psi_{\text{FQS/NFT}}(t) | e^{-iHt} | 0 \rangle^{\otimes 4}\|^2. \quad (32)$$

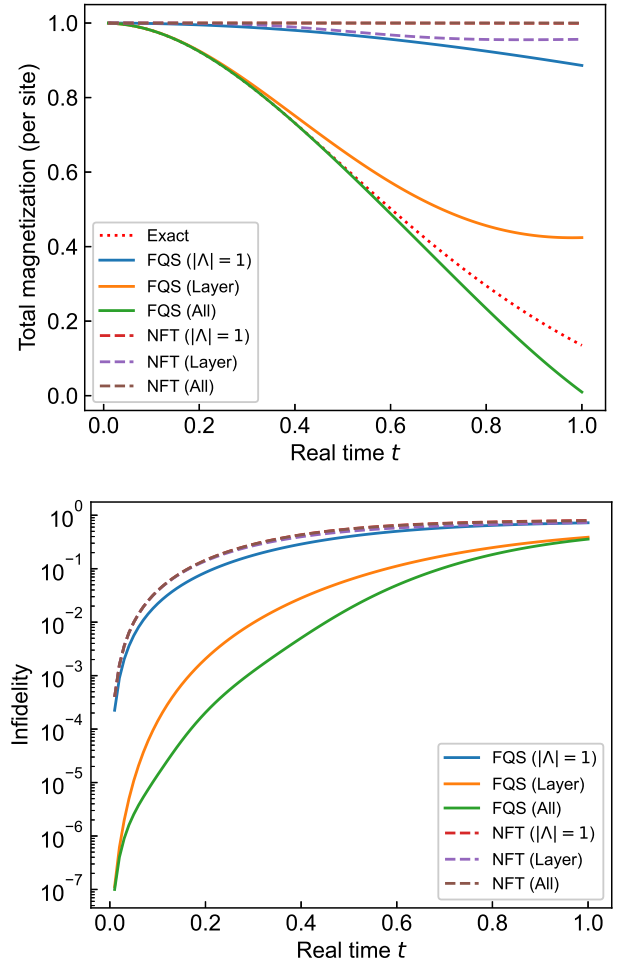


FIG. 4. Dynamics of (Top) total magnetization per site and (Bottom) the infidelity of simulation for 4-qubit 1D Ising model, where the initial states were  $|0\rangle^{\otimes 4}$ . The solid lines and dashed lines represent the results of FQS and NFT, respectively. The red dotted line represents the exact simulation. " $|\Lambda| = 1$ ", "Layer", and "All" denote the level of hardware-efficiency determining the gate set in one optimization problem in Eq. (7).

The NFT method failed to reproduce dynamics of the total magnetization for all three cases, in particular with  $\eta = 1/D$  and 1. Although NFT improved with the use of different initial state [29], FQS still outperformed NFT for all cases. Considering equivalent expressibility of PQC between NFT and FQS, the results imply parameter correlations within a single gate (*intragate* correlation) are more important in real time dynamics than in imaginary time evolution. In addition, although the performance of FQS with  $\eta = 1$  was not necessarily satisfactory, it was drastically improved with group update in FQS with  $\eta = 1/m$  and  $1/D$ . The improvement was due to incorporation of the correlations between multiple gates in one group (*intergate* correlation). In FQS ( $\eta = 1$ ), the divided propagators are uniformly

assigned to all parameterized gates. However, although the error with respect to one divided propagator can be suppressed by fine-grained time steps, the action of each divided propagator may not be sufficiently represented by a single gate update. On the other hands, in FQS with  $\eta = 1/m$  and  $1/D$ , the description of action of one propagator reproduced better by multi-gate update in one optimization.

#### IV. CONCLUSION

In this paper, we proposed a new method called FQS for time evolution simulation with full optimization of a single-qubit gate with respect to its rotational angle and axis. The time evolution is reproduced by sequential optimization of Euclidean norm between target and trial states, instead of the conventional gradient based approach. Because FQS can incorporate correlation among parameters into optimization, it can achieve more accurate simulation. We extended FQS to the excitation-conserving gates that have been widely employed in quantum chemical applications. To verify the performance of the proposed method, we applied it to quantum imaginary time evolution for 1D Heisenberg model and  $H_2$  molecule and confirmed that it effectively led to quantum states that were closer to the true ground states. We also applied FQS to real time evolution of 1D Ising model. Unlike imaginary time evolution, the most hardware-efficient setting with FQS did not reproduce the dynamics with satisfactory accuracy in real time evolution, although the advantage of FQS over other methods was significant. However, its dynamics accuracy was drastically improved when the hardware efficient condition was relaxed with the use of  $\mathcal{O}(m)$  controlled gates,

where  $m$  is the number of qubits.

Although in the present work the gate updating order is fixed from left to right (from the one closest to the input qubits to that closest to the output qubits) of the quantum circuit assuming generality of ansatz and Hamiltonian, the order may not be optimal and there remain rooms for improvement. One way to determine the order is based on the support of the time propagator. These technical improvement may allow the use of FQS in real applications implemented on a bigger size circuit; for instance, calculation of broad vibrational absorption spectra of floppy molecules [33], simulation of short time molecular dynamics observed by femto-second time-resolved spectroscopy [34]. Lastly note that, other than time evolution simulation, FQS is applicable to general optimization problems whose objective functions are given by Euclidean norm between a target state and a trial state of a PQC. Therefore, an improved FQS may also be potentially applicable to such optimization problems in a practical level.

#### V. ACKNOWLEDGEMENTS

H.C.W. was supported by JSPS Grant Numbers 20K03885 and 20H05518, and JST PRESTO Grant number JPMJPR17GC. E.K was supported by JSPS Grant Number 20K14388 and JST PRESTO Grant number JPMJPR2011. In addition, H.C.W., E.K., M.S. and N.Y. were supported by the MEXT Quantum Leap Flagship Program Grant Number JPMXS0118067285 and JPMXS0120319794. We would like to thank Dr. Shumpei Uno, Dr. Yohichi Suzuki, and Dr. Antonio Mezzacapo, for technical discussion, as well as Dr. Michael Lubasch for pointing out details in [27].

- 
- [1] E. Charron and A. Suzor-Weiner, Femtosecond dynamics of nai ionization and dissociative ionization, *J. Chem. Phys.* **108**, 3922 (1998).
  - [2] T. Yonehara, K. Hanasaki, and K. Takatsuka, Fundamental approaches to nonadiabaticity: Toward a chemical theory beyond the born–oppenheimer paradigm, *Chem. Rev.* **112**, 499 (2012).
  - [3] A. Y. Kitaev, Quantum measurements and the abelian stabilizer problem, arXiv:quant-ph/9511026 (1995).
  - [4] B. P. Lanyon, J. D. Whitfield, G. G. Gillett, M. E. Goggin, M. P. Almeida, I. Kassal, J. D. Biamonte, M. Mohseni, B. J. Powell, M. Barbieri, *et al.*, Towards quantum chemistry on a quantum computer, *Nat. Chem.* **2**, 106 (2010).
  - [5] A. Peruzzo, J. McClean, P. Shadbolt, M.-H. Yung, X.-Q. Zhou, P. J. Love, A. Aspuru-Guzik, and J. L. O’Brien, A variational eigenvalue solver on a photonic quantum processor, *Nat. Commun.* **5**, 1 (2014).
  - [6] J. R. McClean, J. Romero, R. Babbush, and A. Aspuru-Guzik, The theory of variational hybrid quantum-classical algorithms, *New J. Phys.* **18**, 023023 (2016).
  - [7] J. Tilly, H. Chen, S. Cao, D. Picozzi, K. Setia, Y. Li, E. Grant, L. Wossnig, I. Rungger, G. H. Booth, *et al.*, The variational quantum eigensolver: a review of methods and best practices, arXiv preprint arXiv:2111.05176 (2021).
  - [8] S. McArdle, T. Jones, S. Endo, Y. Li, S. C. Benjamin, and X. Yuan, Variational ansatz-based quantum simulation of imaginary time evolution, *npj Quantum Inf.* **5**, 1 (2019).
  - [9] M. Motta, C. Sun, A. T. Tan, M. J. O’Rourke, E. Ye, A. J. Minnich, F. G. Brandão, and G. K.-L. Chan, Determining eigenstates and thermal states on a quantum computer using quantum imaginary time evolution, *Nat. Phys.* **16**, 205 (2020).
  - [10] A. Kandala, A. Mezzacapo, K. Temme, M. Takita, M. Brink, J. M. Chow, and J. M. Gambetta, Hardware-efficient variational quantum eigensolver for small molecules and quantum magnets, *Nature* **549**, 242 (2017).
  - [11] C. Hempel, C. Maier, J. Romero, J. McClean, T. Monz, H. Shen, P. Jurcevic, B. P. Lanyon, P. Love, R. Babbush,

- A. Aspuru-Guzik, R. Blatt, and C. F. Roos, Quantum chemistry calculations on a trapped-ion quantum simulator, *Phys. Rev. X* **8**, 031022 (2018).
- [12] A. Kandala, K. Temme, A. D. Córcoles, A. Mezzacapo, J. M. Chow, and J. M. Gambetta, Error mitigation extends the computational reach of a noisy quantum processor, *Nature* **567**, 491 (2019).
- [13] Y. Nam, J.-S. Chen, N. C. Pienti, K. Wright, C. Delaney, D. Maslov, K. R. Brown, S. Allen, J. M. Amini, and J. a. Apisdorf, Ground-state energy estimation of the water molecule on a trapped-ion quantum computer, *npj Quantum Inf.* **6**, 1 (2020).
- [14] J. Tilly, G. Jones, H. Chen, L. Wossnig, and E. Grant, Computation of molecular excited states on ibm quantum computers using a discriminative variational quantum eigensolver, *Phys. Rev. A* **102**, 062425 (2020).
- [15] A. Eddins, M. Motta, T. P. Gujarati, S. Bravyi, A. Mezzacapo, C. Hadfield, and S. Sheldon, Doubling the size of quantum simulators by entanglement forging, *arXiv:2104.10220* (2021).
- [16] Q. Gao, H. Nakamura, T. P. Gujarati, G. O. Jones, J. E. Rice, S. P. Wood, M. Pistoia, J. M. Garcia, and N. Yamamoto, Computational investigations of the lithium superoxide dimer rearrangement on noisy quantum devices, *J. Phys. Chem. A* **125**, 1827 (2021).
- [17] Q. Gao, G. O. Jones, M. Motta, M. Sugawara, H. C. Watanabe, T. Kobayashi, E. Watanabe, Y.-y. Ohnishi, H. Nakamura, and N. Yamamoto, Applications of quantum computing for investigations of electronic transitions in phenylsulfonyl-carbazole tadf emitters, *npj Comput. Mater.* **7**, 1 (2021).
- [18] K. Yeter-Aydeniz, R. C. Pooser, and G. Siopsis, Practical quantum computation of chemical and nuclear energy levels using quantum imaginary time evolution and lanczos algorithms, *npj Quantum Inf.* **6**, 1 (2020).
- [19] H. Ma, M. Govoni, and G. Galli, Quantum simulations of materials on near-term quantum computers, *npj Comput. Mater.* **6**, 1 (2020).
- [20] S.-N. Sun, M. Motta, R. N. Tazhigulov, A. T. Tan, G. K.-L. Chan, and A. J. Minnich, Quantum computation of finite-temperature static and dynamical properties of spin systems using quantum imaginary time evolution, *PRX Quantum* **2**, 010317 (2021).
- [21] S. Sim, P. D. Johnson, and A. Aspuru-Guzik, Expressibility and entangling capability of parameterized quantum circuits for hybrid quantum-classical algorithms, *Adv. Quantum Technol.* **2**, 1900070 (2019).
- [22] M. Cerezo, A. Arrasmith, R. Babbush, S. C. Benjamin, S. Endo, K. Fujii, J. R. McClean, K. Mitarai, X. Yuan, L. Cincio, *et al.*, Variational quantum algorithms, *Nat. Rev. Phys.* , 1 (2021).
- [23] K. Bharti, A. Cervera-Lierta, T. H. Kyaw, T. Haug, S. Alperin-Lea, A. Anand, M. Degroote, H. Heimonen, J. S. Kottmann, T. Menke, *et al.*, Noisy intermediate-scale quantum (nisq) algorithms, *arXiv:2101.08448* (2021).
- [24] K. M. Nakanishi, K. Fujii, and S. Todo, Sequential minimal optimization for quantum-classical hybrid algorithms, *Phys. Rev. Research* **2**, 043158 (2020).
- [25] M. Ostaszewski, E. Grant, and M. Benedetti, Structure optimization for parameterized quantum circuits, *Quantum* **5**, 391 (2021).
- [26] H. C. Watanabe, R. Raymond, Y.-y. Ohnishi, E. Kaminishi, and M. Sugawara, Optimizing parameterized quantum circuits with free-axis selection, *arXiv:2104.14875* (2021).
- [27] M. Benedetti, M. Fiorentini, and M. Lubasch, Hardware-efficient variational quantum algorithms for time evolution, *Phys. Rev. Research* **3**, 033083 (2021).
- [28] K. Mitarai and K. Fujii, Methodology for replacing indirect measurements with direct measurements, *Phys. Rev. Research* **1**, 013006 (2019).
- [29] K. Wada, R. Raymond, Y.-y. Ohnishi, E. Kaminishi, M. Sugawara, N. Yamamoto, and H. C. Watanabe, Simulating time evolution with fully optimized single-qubit gates, *arXiv preprint arXiv:2111.05538* (2021).
- [30] K. Wharton and D. Koch, Unit quaternions and the bloch sphere, *J. Phys. A Math.* **48**, 235302 (2015).
- [31] M. S. ANIS, H. Abraham, AduOffei, R. Agarwal, G. Agliardi, M. Aharoni, I. Y. Akhalwaya, G. Aleksandrowicz, T. Alexander, M. Amy, *et al.*, Qiskit: An open-source framework for quantum computing (2021).
- [32] B. T. Gard, L. Zhu, G. S. Barron, N. J. Mayhall, S. E. Economou, and E. Barnes, Efficient symmetry-preserving state preparation circuits for the variational quantum eigensolver algorithm, *npj Quantum Inf.* **6**, 1 (2020).
- [33] V. Engel, R. Schinke, S. Hennig, and H. Metiu, A time-dependent interpretation of the absorption spectrum of ch3ono, *The Journal of Chemical Physics* **92**, 1 (1990).
- [34] A. H. Zewail, Femtochemistry: Atomic-scale dynamics of the chemical bond, *The Journal of Physical Chemistry A* **104**, 5660 (2000).